Molecular Dynamics Simulation of Unsaturated Lipid Bilayers at Low Hydration: Parameterization and Comparison with Diffraction Studies

Scott E. Feller,* Daxu Yin,# Richard W. Pastor,* and Alexander D. MacKerell, Jr.#
*Biophysics Laboratory, Center for Biologics Evaluation and Research, Food and Drug Administration, Rockville, Maryland 20852-1448, and #Department of Pharmaceutical Sciences, School of Pharmacy, University of Maryland at Baltimore, Baltimore, Maryland 21201 USA

ABSTRACT A potential energy function for unsaturated hydrocarbons is proposed and is shown to agree well with experiment, using molecular dynamics simulations of a water/octene interface and a dioleoyl phosphatidylcholine (DOPC) bilayer. The simulation results verify most of the assumptions used in interpreting the DOPC experiments, but suggest a few that should be reconsidered. Comparisons with recent results of a simulation of a dipalmitoyl phosphatidylcholine (DPPC) lipid bilayer show that disorder is comparable, even though the temperature, hydration level, and surface area/lipid for DOPC are lower. These observations highlight the dramatic effects of unsaturation on bilayer structure.

INTRODUCTION

Although computer simulation of lipid bilayers by molecular dynamics methods is receiving ever increasing attention (for recent reviews, see Merz and Roux, 1996; Pastor, 1994; Tobias et al., 1997), the field is still at a relatively early stage. One measure of this is that while there well over 100 different lipids in biological membranes (Gennis, 1989), most simulations to date have focused on a relatively narrow group of saturated phosphatidylcholines. This is primarily because of the ready availability of detailed experimental data for bilayers composed of these lipids, including equilibrium and dynamic NMR studies (Seelig and Macdonald, 1987; Brown et al., 1990; Douliez et al., 1995) and diffraction data on the crystal (Pascher et al., 1992), gel (Tristram-Nagle et al., 1993), and liquid crystal phases (Nagle et al., 1996). Such data are a natural touchstone for simulations and are often used to develop the initial conditions for the trajectories. It has also been an important check of methodology that different groups using different programs and different potential energy parameters have obtained qualitatively similar results from their simulations.

It is clear, nevertheless, that to model biological membranes, a mix of lipids must be available, especially those with unsaturated chains. To understand why, recall that a biologically active membrane maintains a thickness of ~40 Å and a fluidity characteristic of the liquid crystal (L_α) or melted state. The length condition is met by chain lengths in the range of 16–22 carbons. Temperatures of the gel-to-liquid crystal phase transition (T_m) of bilayers composed of saturated chains of these lengths, however, are above typical physiological temperatures (e.g., T_m = 41.5°C for DPPC; for an extensive compilation of such data, see Small, 1986). Unsaturation lowers T_m, enabling the bilayer to maintain its size, fluidity, and compressibility at physiological temperatures. In addition to lowering T_m, unsaturated lipids play numerous specific roles in specialized membranes (Brown, 1994; Holte et al., 1995, 1996; Litman and Mitchell, 1996).

This paper reports a molecular dynamics (MD) simulation of dioleoyl phosphatidylcholine (DOPC) with 5.36 waters/lipid, and the required parameterization of the atoms associated with an alkene group. Even though biological membranes are typically in excess water (>15 waters/lipid), this system at low hydration was chosen to compare simulation data with the detailed diffraction results of Wiener and White (1991, 1992).

By way of outline, the following section first describes the methods used in the parameterization of the double bond. Particular care was taken to ensure that the new parameters were consistent with the CHARMM22 lipid parameter set (Schlenkrich et al., 1996). The Methods section continues with a description of the initial conditions and protocol used for MD simulations of the octene/water interface and the DOPC bilayer. Results are then presented for various properties of the model compounds used in the parameterization and the surface tension of the water/octene interface. After a general description of the simulation of the DOPC bilayer, the structure is quantified in three ways: 1) the distributions of the total atomic density and that of groups of atoms, including a comparison with experiment; 2) the order parameters of the CH bond vectors, with a comparison with those from recent simulations of dipalmitoyl phosphatidylcholine (DPPC) lipid bilayers (Feller et al., 1997); 3) preliminary results of a comparison of the double bond/water separation with that of water/C9-C10 from the aforementioned DPPC simulation.

Received for publication 12 February 1997 and in final form 4 August 1997.

Address reprint requests to Dr. Richard Pastor, Biophysics Laboratory, Center for Biologics Evaluation and Research, Food and Drug Administration, 1401 Rockville Pike, Rockville, MD 20852-1448. Tel.: 301-435-2035; Fax: 301-496-4684; E-mail: rwpastor@deimos.cber.nih.gov.

Address for supplementary material to Prof. Alexander MacKerell, Jr., Department of Pharmaceutical Sciences School of Pharmacy, University of Maryland, 20 North Pine St., Baltimore, MD 21201. Tel.: 410-706-7442; Fax: 410-706-0346; E-mail: alex@mmiris.ab.umd.edu. Supplementary material is also available on the web site http://www.pharmacy.ab.umd.edu/~alex/.

0006-3495/97/11/2269/11 $2.00

METHODS

Parameterization

Empirical force-field parameters for the alkenes used in the present study were developed to be consistent with the CHARMM22 all-hydrogen parameters for lipids (Schlenkrich et al., 1996). Internal parameters associated with the bond, angle, Urey-Bradley, improper, and dihedral terms in the CHARMM potential energy function (Brooks et al., 1983) were optimized to reproduce experimental and *ab initio* data on geometries, vibrational spectra, and torsional rotation surfaces. Partial atomic charges were optimized to reproduce minimum interaction energies and geometries between selected model compounds and water from HF/6-31G(d) level calculations. Lennard-Jones (LJ) parameters were optimized by applying a new procedure that uses minimum interaction energies and geometries from *ab initio* calculations between the model compounds and helium or neon (Yin and MacKerell, 1996) and experimental pure solvent properties (Yin and MacKerell, 1997); model compounds used for this study were ethene, propene, *cis* and *gauche* 1-butene, and *cis* and *trans* 2-butene.

Molecular mechanics calculations were carried out with version 24 of the program CHARMM (Brooks et al., 1983). Infinite nonbond list cutoffs were adopted for gas-phase evaluations, and minimizations were extended to an RMS gradient of zero. Monte Carlo (MC) calculations were performed with the program BOSS (Jorgensen, 1994), with the Lennard-Jones combining rules converted to those used in CHARMM. Nonbond interactions were truncated at 9.5 Å, with a cubic smoothing function used over the 8.5–9.5-Å region. Step sizes in the MC calculations were adjusted to yield an acceptance ratio of ~40%. Geometries used in the MC calculations were the gas phase-optimized structures, and only the dihedral angles were treated as variables. Systems were equilibrated for 1 M configurations, and averages were collected over the next 3 M configurations.

Ab initio

Calculations were performed with Gaussian94 (Frisch et al., 1994) at the HF/6-31G(d) level of theory, except where specified. Geometry optimizations were to the default tolerances, and frequencies were obtained analytically. *Ab initio* HF/6-31G(d) frequencies were scaled by 0.9 (Florián and Johnson, 1994). Interactions with water were evaluated with the internal geometries of the monomers fixed and only the interaction distance optimized. These calculations were performed with only a single water molecule or rare gas atom present.

Simulations

MD simulations of a 1-octene/water interface and of a DOPC lipid bilayer were carried out with the final version of the alkene parameters. The parameters for the saturated carbons, the lipid headgroup, and the water were taken from the CHARMM22 all-hydrogen parameter set for lipids (Schlenkrich et al., 1996). The octene/water system (62 octene and 560 water molecules) was simulated at 25°C for 100 ps, starting from an initial configuration obtained from a previously published water/octane system (Feller et al., 1996). The DOPC system consisted of 72 lipids and 386 water molecules (5.36 waters/lipid) at a surface area of 59.3 $Å^2$/lipid and a temperature of 23°C; as already noted in the Introduction, these conditions correspond to those studied experimentally. The initial conditions were generated from conformations of individual saturated lipids (results of a Monte Carlo simulation of DPPC in a mean field; Hardy and Pastor, 1994) by first changing the dihedral angle at the 9–10 position to *cis*, and then adding two more carbons in the *trans* state to the end of each fatty acid chain. Random sampling of the resulting conformations was used to select 72 lipids, which were packed into the simulation cell and hydrated to the level determined by experiment. Both the octene/water and DOPC simulations were carried out in the NPAT ensemble: fixed particle number; fixed surface area (x and y dimensions of the tetragonal periodic cell); a variable z dimension that fluctuates to maintain a constant normal pressure of 1 atmosphere (Feller et al., 1995; Zhang et al., 1995); and constant temperature (Hoover, 1985). All bonds involving hydrogen atoms were held fixed with the SHAKE algorithm (Ryckaert et al., 1977). A 2-fs time step was employed with the leapfrog Verlet integration scheme. Lennard-Jones interactions were truncated smoothly over the region from 10 to 12 Å. Coulombic interactions were evaluated with the particle mesh Ewald summation technique (Essmann et al., 1995), using a real space cutoff distance of 12 Å, a screening parameter of 0.230 $Å^{-1}$, and an fft grid density of 1 $Å^{-1}$. The simulation was carried out for 1.5 ns.

For comparison purposes, selected results on DPPC are presented. These simulations were carried out with the same boundary conditions, potential energy function, time step, and model building procedure described here. They differed from the present DOPC simulations in that they were carried out at a higher temperature (50°C) and hydration level (> 25 waters/lipid). Full details are reported elsewhere (Feller et al., 1997).

RESULTS

Parameterization

This subsection describes the optimization of internal and Lennard-Jones parameters and charges, along with the predominant method used to determine them. We emphasize, however, that the actual process was iterative; e.g., charges derived from water-model compound interactions were adjusted after readjustment of the Lennard-Jones parameters.

Optimization of the equilibrium values of the internal parameters was based primarily on the reproduction of experimental gas phase geometries. Overall RMS differences between the empirical and gas phase structures for the bond lengths and bond angles are 0.008 Å and 0.7°, respectively. Direct comparison of the data is included in Table S1 of the supplemental material. Given that the largest differences are 0.012 Å for the bond lengths and −0.9° for the bond angles, the present parameters adequately reproduce the experimental geometries. Reproduction of vibrational spectra dominated the optimization of the internal parameter force constants. Both gas phase experimental and *ab initio* data were used (the *ab initio* data allow for clarification of the assignment of the vibrational frequencies with respect to the internal degrees of freedom). RMS differences between experimental and empirical vibrational spectra are 51, 94, 50, 56, 61, and 44 cm^{-1} for ethene, propene, *cis*-2-butene, *cis*-1-butene, *trans*-2-butene, and *gauche*-1-butene, respectively. The largest disagreement with experiment occurs with propene. This is due to emphasizing the fit for the butenes over propene, because the former are better models for the double bonds occurring in lipids. Full optimization of propene led to an RMS difference of 59 cm^{-1}. Tables S2 to S7 of the supplemental material compare the vibrational results for all of the model compounds. Dihedral parameters were also adjusted to reproduce the relative energies of selected conformers of 1- and 2-butene. Results presented in Table 1 show the agreement between the empirical and *ab initio* data for 1-butene to be good. With 2-butene, however, the empirical barrier at 90° is significantly lower than the *ab initio* data (i.e., 31.2 versus 110.2 kcal/mol). The lower empirical value was selected to reproduce the shape of the energy surface in the vicinity of the minima at 0° (see Table

TABLE 1 Relative energies of selected conformers of 1-butene and 2-butene from the empirical and *ab initio* calculations

	Empirical	*Ab initio*
1-Butene;		
C=C—C—C		
0.0	1.39	1.35
60.0	2.61	2.66
120.0	0.01	0.00
125.8	0.00	—
180.0	1.90	2.28
2-Butene;		
C—C=C—C		
180.0	0.00	0.00
170.0	1.24	1.45
160.0	4.83	5.81
90.0	31.20	110.10
20.0	6.34	7.12
10.0	3.05	3.09
0.0	1.97	1.75

TABLE 2 Comparison of the experimental and simulated heats of vaporization and molecular volumes of the alkene model compounds

	Heats of vaporization	Molecular volume
Ethene		
Exp.*	3.25	81.8
1.5M	3.26 ± 0.01	81.8 ± 0.3
3.0M	3.23 ± 0.01	81.8 ± 0.2
Propene		
Exp.*	4.41	114.9
1.5M	4.37 ± 0.02	115.4 ± 0.5
3.0M	4.34 ± 0.01	116.2 ± 0.3
1-butene		
Exp.*	5.26	148.9
1.5M	5.13 ± 0.02	154.0 ± 0.5
3.0M	5.12 ± 0.02	154.8 ± 0.3
2-butene(*trans*)		
Exp.*	5.46	148.3
1.5M	5.41 ± 0.02	153.3 ± 0.6
3.0M	5.42 ± 0.02	153.1 ± 0.4
2-butene(*cis*)		
Exp.*	5.57	145.0
1.5M	5.70 ± 0.02	145.8 ± 0.6
3.0M	5.67 ± 0.02	146.4 ± 0.4

Simulated results are included for 1.5 and 3.0 million (M) steps of Monte Carlo sampling.
*Smith, B. D. 1986. Thermodynamic Data for Pure Compounds, Part A. Elsevier, New York.

1) and is sufficiently large to ensure that rotation does not occur in MD simulations at room temperature. The level of agreement of the present parameters with the target data is similar to that observed with the MM3 force field (Allinger et al., 1990). Explicit optimization of the model compounds in CHARMM allows for a level of agreement comparable to that by MM3 while using a much simpler potential energy function.

Optimization of the LJ parameters emphasized both the relative values of the radii and well depths for the individual atom types and the absolute values of those terms (Yin and MacKerell, 1997). The relative values were obtained by reproducing relative minimum interaction energies and geometries between helium or neon and ethene or propene, based on *ab initio* calculations at the MP3/6-311++G(3d, 3p) level of theory. This level of theory, however, is not adequate for obtaining the absolute value of the parameters. Thus experimental heats of vaporization and molecular volumes for pure solvents are also included as goal data. Consistent with trends observed for alkanes (Yin and MacKerell, 1997), the *ab initio* and empirical geometries are in good agreement, whereas the energies differ significantly (Fig. S1 and Table S8 of the supplemental material). The level of agreement between the calculated and experimental pure solvent properties is very good (Table 2). The largest discrepancies occur with 1-butene. With this compound, as well as with 2-butene, the LJ parameters were transferred directly from ethene and propene. Although further optimization of the LJ parameters could have been performed on these compounds, the level of agreement with experiment was deemed adequate. Of note is the agreement between simulation and experiment for *cis*- and *trans*-2-butene, because these compounds best model the double bonds occurring in lipid aliphatic chains.

Partial atomic charges were optimized based on the reproduction of minimum interaction energies and geometries between water and ethene or propene (Reiher, 1985; Jorgensen, 1986). The *ab initio* energies were scaled by 1.16 before their use as target data (MacKerell and Karplus, 1991). Interaction orientations, and a comparison of the empirical and *ab initio* minimum interaction energies and geometries, are shown in Fig. S1 and Table S9 of the supplemental material. For ethene the empirical energies are in good agreement with the *ab initio* data. With propene, however, the first two in-plane interaction orientations are somewhat less favorable, and interaction three, which is out of plane with the water hydrogen directed toward the carbon atom, is too favorable. This discrepancy is associated with the interaction of the water molecule in the plane of the double bond versus the out-of-plane interaction, which occurs directly with the *p* orbitals. Problems with interactions involving the *p* orbitals are also seen in the minimum interaction distances with water in orientation three and for helium-to-ethene interaction orientations three and four (Table S8). These problems are associated with the use of spherical atoms in the CHARMM potential energy function. A final check of the charge distribution was based on the dipole moment of propene. The empirical partial atomic charges yield a value of 0.526, which compares with an HF/6-31G(d) value of 0.302 and an experimental gas phase value of 0.366 (*Handbook of Chemistry and Physics*). Overestimation of the dipole moment is consistent with that occurring with the TIP3P water model (Jorgensen et al.,

1983) and is required because of the omission of an explicit term for electrostatic polarizability in the present potential energy function. The optimized partial atomic charges are shown in Fig. 1.

The final alkene parameters are listed in Table 3.

Simulation of water/octene

The water/octene simulation served as a test of the hydrophobic interactions between water and an alkene. The surface tension, γ, was evaluated from the difference between normal and tangential components of the pressure tensor (Zhang et al., 1995); it equaled 41.1 ± 3.4 dyn/cm, in good agreement with the experimental value of 46.6 dyn/cm (Nakahara and Masamoto, 1990). The present parameter set yields γ = 46.6 ± 2.4 dyn/cm for water/octane (Feller et al., 1996), which is also ~5 dyn/cm less than experiment (51.7 dyn/cm). Hence the calculated reduction in surface tension upon the addition of unsaturation is reproduced very well. As a note of caution, there are unresolved issues in the parameterization of water/hydrocarbon systems. Notably, the water/vapor surface tension for these parameters and Ewald summation is 52.7 ± 1.5 dyn/cm, or ~20 dyn/cm lower than experiment (Feller et al., 1996). Consequently, the experimentally observed 25 dyn/cm difference in surface tensions between water/vapor and water/octene is not reproduced. This discrepancy may be associated with the fact that TIP3P water is a better liquid phase than gas phase model, so that water/vapor surface tensions should not be expected to be as close to experiment as water/alkane or water/alkene surface tensions.

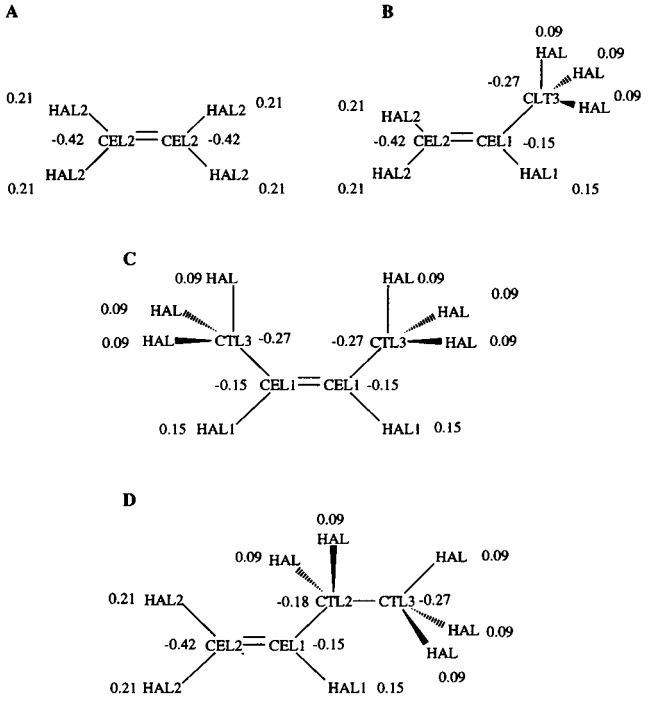

FIGURE 1 Partial atomic charges and atom types for the model compounds. (*A*) Ethene. (*B*) Propene. (*C*) 2-Butene. (*D*) 1-Butene.

Simulation of a DOPC bilayer

Equilibration and general features

Turning to DOPC, Fig. 2 shows that 0.5 ns of equilibration was required to achieve convergence of the internal energy and cell parameters. The trajectory from 0.5 to 1.5 ns was subsequently used for all analysis. The average height of the simulation cell, which corresponds to the experimental D-spacing, equaled 49.1 ± 0.1 Å (the standard error was determined from the 200-ps block averages). The preceding D-spacing is statistically indistinguishable from the experimental value of 49.1 ± 0.3 Å.

The surface tension, calculated from the simulation via the anisotropy in the pressure tensor, equaled 0 ± 3 dyn/cm. Recently we suggested that the surface tension observed in an MD simulation may differ from that expected of macroscopic membranes, and we demonstrated explicit size dependence on the observed tension (Feller et al., 1996). The existence of this "microscopic" surface tension was explained in terms of restricting undulations via periodic boundary conditions. If we assume that the potential energy parameters are accurate, the zero surface tension obtained here leads to two possible conclusions: 1) the macroscopic surface tension of DOPC is zero and the effect of undulations is negligible (because of the very low hydration); 2) the macroscopic surface tension is nonzero, but was not observed because the surface area of 59.3 Å^2/lipid was too small (as area is reduced, the lateral pressure becomes less negative and the surface tension decreases).

Fig. 3 shows a slab of the lipid bilayer taken from the MD simulation at 1.0 ns (midway through the production run). At this low hydration level of 5.4 waters/lipid, there is very close contact between bilayers, and even partial interdigitation of opposing headgroups. Nevertheless, the bilayer interior is in a fluid, as opposed to gel, state.

Density profiles: description

The diffraction studies of Wiener and White (1991, 1992) yield the absolute x-ray and neutron scattering densities as a function of position along the bilayer normal (z axis). Comparison between the simulation and experiment was made by dividing the simulation cell into 490 bins and calculating the electron density (using the atomic numbers of the atoms) or neutron scattering density (using the values in Wiener and White, 1992b). The bins were ~0.1 Å wide and fluctuated slightly in volume because the height of the simulation cell fluctuated. Fig. 4 (*top*, neutron; *bottom*, x-ray) plots the scattering density profiles from both experiment and simulation along the bilayer normal. The agreement is very good throughout the interior of the bilayer, with both the widths and the depths of the trough region reproduced by the simulation. The heights and widths of the

TABLE 3 Alkene parameters

Bonds				K_b (kcal/mol/Å^2)	b_0 (Å)	
CEL1	CEL1			440.00	1.3400	
CEL1	CEL2			500.00	1.3420	
CEL1	CTL2			365.00	1.5020	
CEL1	CTL3			383.00	1.5040	
CEL2	CEL2			510.00	1.3300	
HAL1	CEL1			360.50	1.1000	
HAL2	CEL2			365.00	1.1000	
Bond angles				K_θ (kcal/mol/degree^2)	θ_0 (degree)	
CEL1	CEL1	CTL3		48.00	123.50	
CEL1	CEL1	CTL2		48.00	123.50	
CEL1	CTL2	CTL3		32.00	112.20	
CEL1	CTL2	CTL2		32.00	112.20	
CEL2	CEL1	CTL2		48.00	126.00	
CEL2	CEL1	CTL3		47.00	125.20	
HAL	CTL2	CEL1		45.00	111.50	
HAL	CTL3	CEL1		42.00	111.50	
HAL1	CEL1	CEL1		52.00	119.50	
HAL1	CEL1	CEL2		42.00	118.00	
HAL1	CEL1	CTL2		40.00	116.00	
HAL1	CEL1	CTL3		22.00	117.00	
HAL2	CEL2	CEL1		45.00	120.50	
HAL2	CEL2	CEL2		55.50	120.50	
HAL2	CEL2	HAL2		19.00	119.00	
Dihedrals				K_ϕ (kcal/mol)	n	δ (degree)
CEL1	CEL1	CTL3	HA	0.03	3	0.00
CEL2	CEL1	CTL2	CTL3	0.50	3	0.00
CEL2	CEL1	CTL2	HA	0.12	3	0.00
CEL2	CEL1	CTL3	HA	0.05	3	180.00
CTL3	CEL1	CEL2	HAL2	5.20	2	180.00
HAL1	CEL1	CEL2	HAL2	5.20	2	180.00
HAL1	CEL1	CTL2	HA	0.87	3	0.00
HAL1	CEL1	CTL2	CTL3	0.12	3	0.00
HAL1	CEL1	CTL3	HA	0.34	3	0.00
HAL2	CEL2	CEL1	CTL2	5.20	2	180.00
X	CEL1	CEL1	X	5.20	2	180.00
X	CEL2	CEL2	X	4.90	2	180.00
Impropers				K_ω (kcal/mol)		ω_0 (degree)
HAL2	HAL2	CEL2	CEL2	3.00		0.00
Lennard-Jones				E_{min} (kcal/mol)	$R_{min}/2$ (Å)	
CEL1				−0.068	2.09	
CEL2				−0.064	2.08	
HAL1				−0.031	1.25	
HAL2				−0.026	1.26	

Refer to Fig. 1 for atom names. X denotes wildcard.

headgroup peaks are also in good agreement, although the positions of the simulation peaks are shifted ~1 Å away from the bilayer center. The relatively large scatter and asymmetry in the headgroup regions (i.e., the peaks) compared to the interior are likely due to poorer conformational sampling because of the much slower isomerization rates in the glycerol and phosphatidylcholine segments (Pastor and Feller, 1996).

For a higher resolution description, we follow Wiener and White, who analyzed their DOPC data with a model containing eight independent groups: methyl, methylene, alkene, carbonyl, glycerol, phosphate, choline, and water (Fig. 3 is colored according to this grouping). Using both x-ray and neutron scattering densities in a joint refinement procedure, Wiener and White determined the distribution of each group along the bilayer normal.

The simulated and joint-refinement distributions are plotted in Fig. 5. Table 4 lists values of the average position ($\langle z \rangle$) and width (σ) of each molecular fragment as determined from experiment, and from the simulation using two different methods: method A, a direct calculation with

$$\langle z \rangle = \sum_i p_i z_i \qquad \sigma^2 = \sum_i p_i (z_i - \langle z \rangle)^2 \tag{1}$$

where p_i is the probability of being located in the ith slab; and method B, a fit of the data to a Gaussian (or normal) density used in the joint refinement procedure.

Qualitatively, the agreement for the water and the double-bond distributions, which were determined unambiguously by specific deuteration, is very good (Fig. 5, *top*). Fig. 5 (*bottom*) shows the distributions for the fragments located in

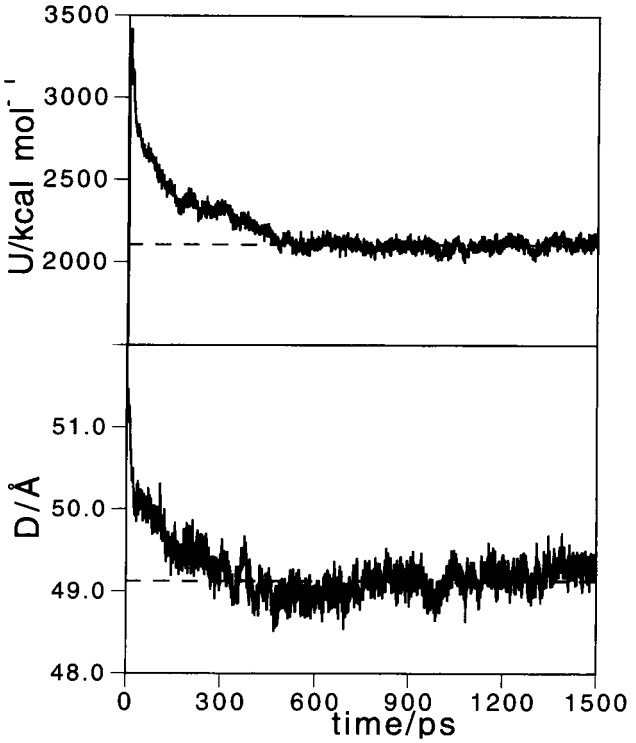

FIGURE 2 Internal energy (*top*) and simulation cell length (or D-spacing) (*bottom*) as a function of time during the simulation of a DOPC bilayer. The dashed lines denote the averages from 500 to 1500 ps; the D-spacings from simulation and experiment (Wiener and White, 1992) are both 49.1 Å.

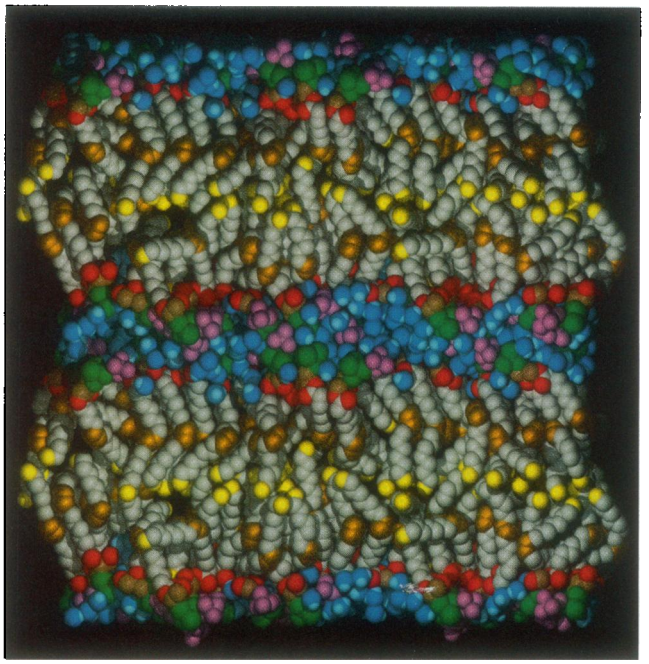

FIGURE 3 A snapshot taken from the 1-ns point in the trajectory, showing the periodic image normal to the bilayer. Atoms are colored according to the grouping developed by Wiener and White (1992b): yellow, chain terminal methyl; gray, chain methylene; copper, alkene carbon; red, carbonyl and ester oxygen; brown, glycerol carbon; green, phosphate; pink, choline; dark blue, water oxygen; light blue, water hydrogen.

the headgroup region (for clarity, only one of the two mirror images is plotted for each group). Whereas the choline and glycerol peaks from the simulation are within 0.4 Å of those from the joint refinement, the carbonyl and phosphate peaks lie ~1 Å further from the center (as might be expected from Fig. 4). The total methyl peak position is close to zero, in agreement with experiment; however, the averages for the top and bottom leaflets are 1.53 and −1.81 Å, respectively. Another potentially interesting discrepancy involves the difference between the carbonyl and glycerol positions: 2.7 Å from the refinement versus 1.6 Å from the simulation.

There is excellent agreement between simulation and joint refinement for the peak widths for all but the methyl groups. In cases of good agreement, the differences in σ obtained from methods A and B are generally less than the differences between the two sides of the bilayer calculated with the same method (Table 4). The skew and kurtosis of these distributions are also close to zero (absolute value $<$ 0.35 in all cases); i.e., they are well approximated as normal. A discrepancy is found at the center of the bilayer, where the joint refinement predicts a more localized methyl density and a corresponding decrease in methylene density. It is possible that some of the difference in simulation and experiment is associated with modeling the methyl density as a single Gaussian distribution. The kurtosis of the simulated distribution is 2.8, an order of magnitude larger than for the other groups; this is consistent with the relatively large differences in σ obtained by methods A and B (Table 4). As noted above, the means of the methyl distributions from the top and bottom leaflets differ by 3.3 Å. Their skew and kurtosis are 1.2 and 1.9, respectively, for the top leaflet, and −0.91 and 2.2 for the bottom leaflet. Hence the small skew of −0.15 for the combined distribution is arguably fortuitous.

Density profiles: statistical analysis

The (albeit small) discrepancies in peak positions could be associated with 1) statistical error in the simulation (e.g., inadequate sampling of the headgroup configurations); 2) incorrect assumptions in the joint refinement procedure (e.g., fitting to normal distributions and thereby ignoring asymmetry) or other experimental errors; 3) a more serious error in the simulation.

To determine whether the differences are statistically significant, the confidence interval of the simulated value must be obtained (we ignore for now statistical errors in the experiment). The confidence interval at level α about a mean, m, with n independent samples is given by

$$m \pm t_{1-\alpha/2} s/\sqrt{n} \qquad (2)$$

where t is the value from the t-distribution, with $n - 1$ degrees of freedom, and s is the sample standard deviation (DeGroot, 1975). If the confidence intervals bracket exper-

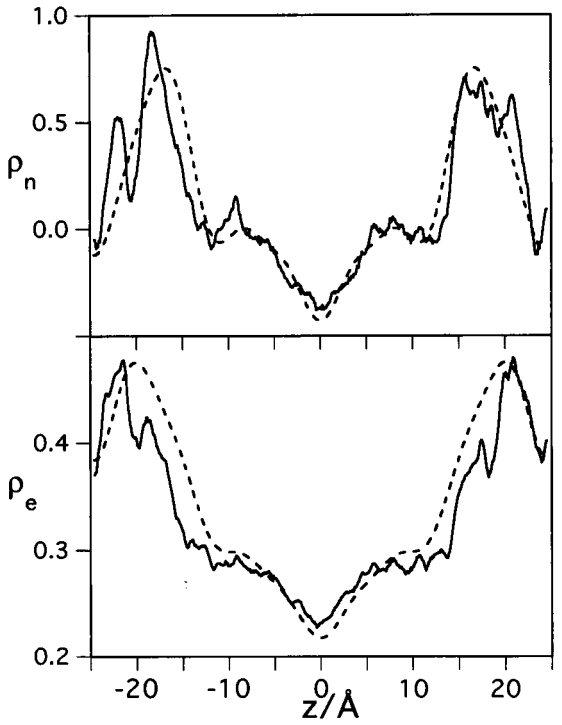

FIGURE 4 Neutron (*top*) and x-ray (*bottom*) scattering density profiles of the DOPC bilayer from simulation (——) and experiment (Wiener and White, 1992) (– – –). Units of density are scattering length per unit length) $\times 10^4$ (*top*) and $e/Å^3$ (*bottom*).

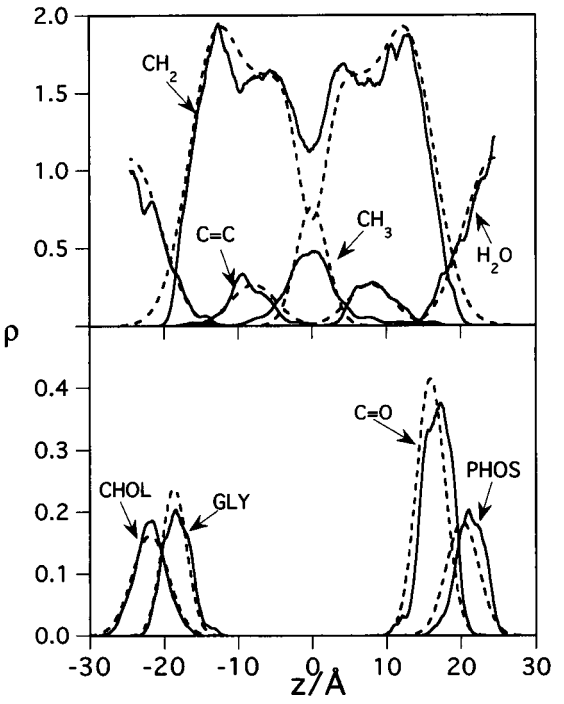

FIGURE 5 Density distributions of DOPC molecular fragments from simulation (——) and joint refinement (Wiener and White, 1992b) (– – –). Distributions shown in the lower panel have been made symmetrical by averaging over both halves of the bilayer. For clarity, only one half of the resulting mirror image is plotted.

iment, the null hypothesis (that the simulated and experimental values are statistically equal) is accepted; if not, it is rejected (i.e., the alternative hypothesis, that there is a difference, is accepted). Hypothesis testing is typically carried out at the 95% ($\alpha = 0.05$) level, which means the confidence interval is set such that on average, 5% of the time the null hypothesis is incorrectly rejected. This is a Type I error. A Type II error occurs when the alternative hypothesis is incorrectly rejected (i.e., a real difference was not discerned). The power is defined as $1 - \beta$, where β is the probability of a Type II error. A relatively large interval (as might be obtained when n is small) is typically associated with low power. When the sample standard deviation is known in advance or when n is large, $t_{0.975}$ can be assumed to equal 1.96.

The primary difficulty in applying Eq. 2 to the present data is that positions of groups are highly correlated, even after 1 ns of simulation. This is partially illustrated in Fig. 6, where the average positions of the phosphate and choline groups on opposite sides of the bilayer show clear periods of correlation, as well as some anticorrelation (e.g., 560 ps). The time scale of dynamics along the bilayer normal is also long compared to the simulation length. For example, individual phosphates traversed a range of 2.9 Å on average, whereas the full range for phosphates was ~10 Å. Consequently, the number of independent samples is not expected to equal the number of lipids (or chains). This nuance, in fact, determines whether the positions of some of the groups agree with experiment. For example, the standard deviation of sample means for the phosphates equaled 1.64 Å. Hence, from Eq. 2, possible 95% confidence intervals are 21.18 ± 0.38 Å ($n = 72$, all lipids independent) and 21.18 ± 3.2 Å ($n = 1$, all lipids completely correlated). The first interval does not bracket the experiment; the second one does, but the power is low.

This paragraph presents an *ad hoc* method for determining the effective number of independent samples, n_{eff}, for each group. Consider again the phosphates, and define the following quantity evaluated from the k nearest neighbors for each lipid:

$$C_k = \left\langle \sum_{j=1}^{k} \delta z_i \delta z_j \right\rangle_i \qquad (3)$$

where $\delta z_i = \langle z_i \rangle - \langle z \rangle_{side}$, and $\langle z_i \rangle$ is the average position of the ith lipid. The correlation of groups with their nearest neighbors, ρ, is defined in analogy to standard statistical nomenclature: $\rho = C_1/s^2$. For the phosphate, the correlation is high and spatially long lived: $C_1 = 0.995$ ($\rho = 0.370$), $C_2 = 0.976$, $C_3 = 0.727$, $C_6 = 0.628$, $C_{12} = 0.385$, and $C_{24} = 0.081$. For the next step we ask the question, "What is the number of samples taken from uncorrelated distributions that yields the same results, on average?" We determined this numerically by sampling from normal distributions with $\sigma = 1.64$ Å, and evaluating C_k by using the

TABLE 4 Value of the average location (as measured from the bilayer center) and width of molecular fragment distributions

	⟨z⟩/Å			σ/Å		
Group	Method A	Method B	Joint refinement	Method A	Method B	Joint refinement
Choline	21.86 (0.09)	21.88 (0.28)	21.89 ± 0.13	2.14 (0.11)	2.11 (0.17)	2.46 ± 0.39
Phosphate	21.18 (0.28)	21.34 (0.47)	20.19 ± 0.08	1.85 (0.19)	1.89 (0.25)	2.18 ± 0.06
Glycerol	18.28 (0.31)	18.36 (0.58)	18.67 ± 0.32	1.85 (0.11)	1.86 (0.10)	1.68 ± 0.22
Carbonyl	16.62 (0.22)	16.91 (0.69)	15.97 ± 0.02	1.92 (0.11)	1.92 (0.11)	1.93 ± 0.04
C=C	8.66 (0.07)	8.49 (0.43)	7.88 ± 0.09	2.82 (0.05)	2.70 (0.18)	3.03 ± 0.11
Methyl	−0.14	−0.22	0.0	4.38	3.17	2.09 ± 0.20

Simulation data were analyzed using Eq. (1) (method A) and by fitting to a Gaussian (method B). The values in parentheses indicate the difference between the two halves of the bilayer. Included are the results of a joint refinement of x-ray and neutron diffraction data by Wiener and White (1992).

absolute value of the sum in brackets. For $n = 4$, we obtain $C_1 = 1.03$ ($\rho = 0.383$), $C_2 = 0.885$, $C_3 = 0.833$; and, for $n = 5$, $C_1 = 0.913$ ($\rho = 0.339$), $C_2 = 0.759$, $C_3 = 0.705$. Hence this simple analysis approximately reproduces the downward trend of the first several points and predicts that n_{eff} is ~4. From Eq. 2, the confidence interval is 21.18 ± 1.6 Å. The results of similar analysis of the other groups are summarized in Table 5. For each case, C_1 was used to estimate n_{eff}. Calculations were carried out separately for each chain, because the correlation for groups on the same lipid was typically large. From this analysis we conclude that simulation and joint refinement agree for the location of peak positions, although the need for longer simulations is evident.

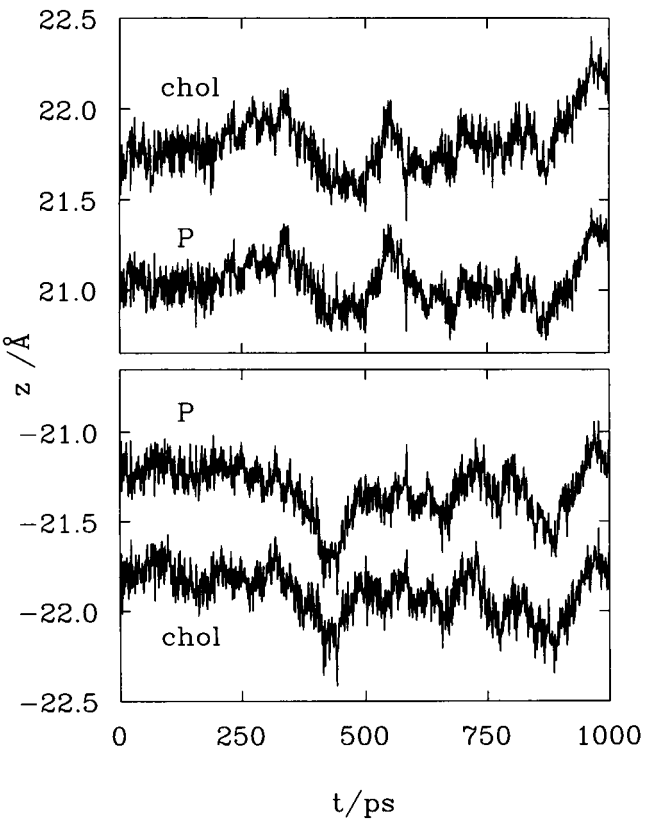

FIGURE 6 Instantaneous headgroup projections along the bilayer normal (averaged over lipids in each leaflet). Note that because of periodic boundary conditions the average choline and phosphate positions from the two leaflets are separated by only 5.4 and 6.9 Å, respectively, and interact strongly.

The values of n_{eff} estimated above are a function of simulation length. For very long simulations, correlations between the average positions among lipids will decrease to zero (despite correlations between instantaneous positions), and the number of independent samples for the headgroup positions will approach the number of lipids. The question of whether groups on the same lipids can be treated as independent samples, even at very long times, remains unresolved.

Finally, we consider the independence of phosphate positions from a 500-ps segment of a recent simulation of fully hydrated DPPC at 50°C at surface area of 62.9 Å^2/lipid (Feller et al., 1997). For this system the analysis just described yields $C_1 = 0.536$, $\rho = 0.370$, $n_{eff} = 10$, and 95% confidence intervals of ± 0.92 Å.

Deuterium order parameters

Deuterium order parameters, obtained from NMR experiments, are often used to probe the structure of lipid bilayer membranes. The order parameter, S_{CD}, is given by

$$S_{CD} = \langle 3/2 \cos^2\theta - 1/2 \rangle \quad (4)$$

where θ is the angle between the CD bond vector and the bilayer normal. The filled symbols in Fig. 7 (*top*) show the simulated values for DOPC. There is a plateau region between C3 and C7 where S_{CD} is ~0.22, followed by a sharp dip at the location of the double bond and its nearest neighbors, and decreasing order at the end of the chains. Although we do not have a direct comparison to experiment, the magnitudes of the C9 and C10 order parameters are very similar to those observed in mixed-chain lipid bilayers (Seelig and Wasepe-Sarcevic, 1978).

As shown in Fig. 7 (*bottom*), the plateau region is similar to that calculated for fully hydrated DPPC at 50°C at surface area of 62.9 Å^2/lipid. In contrast, the order parameters for DPPC simulated at 59.3 Å^2/lipid (the same as in the present DOPC system) are qualitatively higher in this region (Fig. 7,

TABLE 5 Results of the statistical analysis of peak positions

Group	C_1	s/Å	ρ	n_{eff}	⟨z⟩/Å 95% conf. interval	⟨z⟩/Å Joint refinement
Choline	0.409	1.81	0.125	40	21.86 ± 0.56	21.89
Phosphate	0.995	1.64	0.370	4	21.18 ± 1.6	20.19
Glycerol	0.867	1.60	0.339	5	18.28 ± 1.4	18.67
Carbonyl	0.714	1.83	0.213	13	16.62 ± 0.99	15.97
C=C	1.86	2.63	0.270	8	8.66 ± 1.8	7.88
Methyl	4.10	4.13	0.240	10	−0.14 ± 2.6	0.0

C_1 is the covariance of nearest-neighbor positions defined by Eq. 3; s is the standard deviation in the distribution of means; ρ is the correlation, defined as C_1/s^2; n_{eff} is the effective number of independent samples. The final two columns list the 95% confidence intervals for the peak positions for the simulation, and the values derived from joint refinement.

bottom). The DPPC system at 59.3 Å^2/lipid is at a much higher temperature and hydration level, factors that tend to increase disorder, yet the DOPC simulation shows much smaller values of S_{CD}. This comparison suggests a strong relation between disorder, as measured by S_{CD}, and the presence of unsaturation.

Interaction with water

Finally, Fig. 8 compares the density of water around the unsaturated carbon positions as a function of radial distance, along with the same quantity calculated around the C9 and C10 positions of DPPC at A = 62.9 Å^2/lipid. The increased affinity for water of the alkene is clearly evidenced by the presence of a peak in water density compared to the featureless alkane-water density profile. If the DOPC bilayer were fully hydrated (as was the DPPC system), it seems likely that the difference in water densities would be even greater. A more extensive analysis is under way (Feller, manuscript in preparation).

DISCUSSION AND CONCLUSIONS

Atomic-level simulation, with its extremely high spatial resolution, is a powerful tool for determining membrane structure. However, validation of the potential energy function is essential when extending the method to new and complex systems. The potential energy terms for unsaturated hydrocarbons developed in this paper were refined by using a variety of experimental pure solvent properties. They were then independently tested by using a water/octene interface (where the surface tension is a sensitive measure of interaction with water) and a DOPC lipid bilayer at low hydration (where very high-quality diffraction data are available).

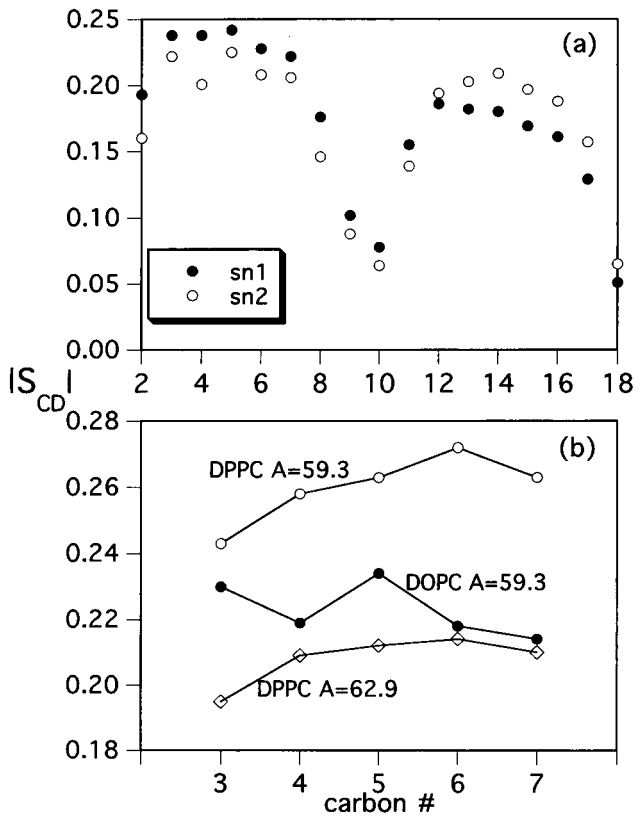

FIGURE 7 Simulated deuterium order parameters as a function of chain position. (*a*) DOPC. (*b*) DOPC and DPPC at two different surface areas (Feller et al., 1997).

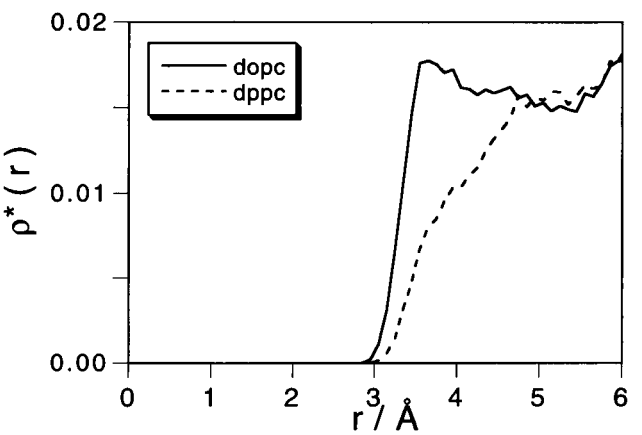

FIGURE 8 Density of water as a function of distance from the C9 or C10 carbon position for DOPC (——) and DPPC (– – –).

Simulations of water/octene and water/octane reproduced the experimentally observed 5 dyn/cm difference in interfacial tensions, a good indication that the parameterization of the alkene group is internally consistent. We suggest that water/hydrocarbon interfacial tensions be considered in the much needed development of water models.

Simulations of DOPC showed very good agreement with experimental densities (Figs. 4 and 5). Although a statistically rigorous comparison is difficult to make because of the high spatial correlation among groups (Fig. 6), the estimated 95% confidence intervals of all group peak positions bracket those derived from a joint refinement of neutron and electron diffraction data (Table 5). Although the method used to determine the effective number of independent lipids is *ad hoc*, it certainly suggests that a reasonable criterion for obtaining tight error bounds for density peaks is that each lipid should sample the full range taken on by the collection of lipids.

Aside from the methyls, simulated peak widths showed excellent agreement with experiment (Table 4); their small kurtosis and skew also help validate assumptions of normality for the distributions. The simulated methyl distribution is broader than the experimental distribution and has a high kurtosis. It does not appear that the methyl density is well modeled by one or even two Gaussians, and it may be of interest to analyze experimental results by using other distributions. Separate experimental evidence for the broad methyl distribution of the simulation can be found from 2D NMR experiments where cross-peaks are observed between methyl groups and the headgroup (K. Gawrisch, personal communication).

The results of the present simulation also agree qualitatively with previous molecular dynamics (Heller et al., 1993; Huang et al., 1994) and Langevin dynamics (Pearce and Harvey, 1993) simulations on unsaturated lipids. The characteristic dip at the double-bond position is reproduced in all studies, even though different boundary conditions, potential functions, and cutoff methods were used. The MD studies were carried out at full hydration, and should not be expected to yield results quantitatively similar to those of the present simulation. For example, the phosphate peak spacing and surface area per lipid determined by Heller et al. for 1-palmitoyl-2-oleoyl phosphatidylcholine (POPC) equaled 17.65 Å and 65.5 Å^2, respectively. As required to maintain a relatively constant density, the surface area is larger and bilayer thickness is smaller than DOPC at low hydration, and the order profile is shifted to lower $|S_{CD}|$.

Several comparisons of DOPC and DPPC were presented. Even though the temperature, hydration level, and surface area/lipid for DOPC are lower than DPPC, the two systems are approximately equally disordered in the bilayer interior (Fig. 7). However, the interaction of the double bond in DOPC with water is significantly stronger than that of the corresponding single bonds in DPPC (Fig. 8). As discussed earlier by Wiener and White (1992b), it is probable that the ability of the unsaturated sites to have relatively favorable interactions with polar groups is important for membrane permeability and for stabilizing complex lipid-protein structures. Both the disorder and the double bond-water interactions are expected to increase markedly as the hydration is raised to more biologically relevant levels. The headgroup region of DOPC appears to be more rigid than that of DPPC, although it is difficult to assign the effect to hydration, surface area, or unsaturation with the present data.

As a methodological point, there has been concern that because Ewald summation imposes long-range correlation, there is a possibility of artificially induced order. Such an effect could be serious for a bilayer at low hydration. Arguments in favor of employing Ewald summation as opposed to spherical methods for bilayers have been presented recently by Tobias et al. (1997) and Feller et al. (1996). It may be of interest to carry out simulations of the present system with other boundary conditions.

It will be necessary at some point to carry out longer simulations of this system to ascertain whether the differences between simulation and experiment listed in Table 4 remain statistically insignificant. If differences are found to be systematic, a more extensive investigation of both the simulation model (e.g., errors in the parameters) and experimental conclusions (e.g., the surface area per lipid) will be warranted. Studies of DOPC at higher hydration are also of interest.

The present validation of the CHARMM potential for bilayers of DOPC allows the simulation of bilayers of biologically relevant mixed chain and polyunsaturated lipids. Because this parameter set is also optimized to maintain compatibility with the protein parameters, a wide range of simulation studies is now feasible.

We thank Peter Munson for helpful discussions on statistics. Computer time for this project was provided in part by the National Cancer Institute Frederick Biomedical Computing Center.

ADM acknowledges financial support from National Institutes of Health grant GM51501-01.

REFERENCES

Allinger, N. L., F. Li, and L. Yan. 1990. Molecular mechanics. The MM3 force field for alkenes. *J. Comp. Chem.* 11:848–867.

Brooks, B. R., R. E. Bruccoleri, B. D. Olafson, D. J. States, S. Swaminathan, and M. Karplus. 1983. CHARMM: a program for macromolecular energy, minimization, and dynamics calculations. *J. Comput. Chem.* 4:187–217.

Brown, M. F. 1994. Modulation of rhodopsin function by properties of the membrane bilayer. *Chem. Phys. Lipids.* 73:159–180.

Brown, M. F., A. Salmon, U. Henriksson, and O. Soderman. 1990. Frequency dependent ^{2}H NMR relaxation studies of small unilamellar phospholipid vesicles. *Mol. Phys.* 69:379–383.

DeGroot, M. H. 1975. Probability and Statistics. Addison-Wesley, Reading, MA.

Douliez, J-P., A. Leonard, and E. J. Dufourc. 1995. Restatement of order parameters in biomembranes: calculation of C-C bond order parameters from C-D quadrupolar splittings. *Biophys. J.* 68:1727–1739.

Essmann, U., L. Perera, M. L. Berkowitz, T. Darden, H. Lee, and L. G. Pedersen. 1995. A smooth particle mesh Ewald method. *J. Chem. Phys.* 103:8577–8593.

Feller, S. E., R. W. Pastor, A. Rojnuckarin, S. Bogusz, and B. R. Brooks. 1996. Effect of electrostatic force truncation on interfacial and transport properties of water. *J. Phys. Chem.* 100:10711–10720.

Feller, S. E., R. M. Venable, and R. W. Pastor. 1997. Computer simulation of a DPPC phospholipid bilayer: structural changes as a function of molecular surface area. *Langmuir.* in press.

Feller, S. E., Y. Zhang, R. W. Pastor, and B. R. Brooks. 1995. Constant pressure molecular dynamics simulation: the Langevin piston method. *J. Chem. Phys.* 103:4613–4621.

Florián, J., and B. G. Johnson. 1994. Comparison and scaling of Hartree-Fock and density functional harmonic force fields. 1. Formamide monomer. *J. Phys. Chem.* 98:3681–3687.

Frisch, M. J., G. W. Trucks, H. B. Schlegel, P. M. W. Gill, B. G. Johnson, M. A. Robb, J. R. Cheeseman, K. Raghavachari, M. A. Al-Laham, V. G. Zakrzewski, J. V. Ortiz, J. B. Foresman, J. Cioslowski, B. B. Stefanov, A. Nanayakkara, M. Challacombe, C. Y. Peng, P. Y. Ayala, W. Chen, M. W. Wong, J. L. Andres, E. S. Replogle, R. Gomperts, R. L. Martin, D. J. Fox, J. S. Binkley, D. J. Defrees, J. Baker, J. J. P. Stewart, M. Head-Gordon, C. Gonzalez, and J. A. Pople. 1996. Gaussian 94. Gaussian, Inc., Pittsburgh, PA.

Gennis, R. B. 1989. Biomembranes, Molecular Structure, and Function. 1989. Springer Verlag, New York.

Hardy, B. J., and R. W. Pastor. 1994. Conformational sampling of hydrocarbon and lipid chains in an orienting potential. *J. Comp. Chem.* 15:208–226.

Heller, H., M. Schaefer, and K. Schulten. 1993. Molecular dynamics simulation of a bilayer of 200 lipids in the gel and liquid-crystal phases. *J. Phys. Chem.* 97:8343–8360.

Holte, L. L., S. A. Peter, T. M. Sinnwell, and K. Gawrisch. 1995. ^{2}H nuclear resonance order parameter profiles suggest a change in molecular shape for phosphatidylcholines containing a polyunsaturated acyl chain. *Biophys. J.* 68:2396–2403.

Holte, L. L., F. Separovic, and K. Gawrisch. 1996. Nuclear magnetic resonance investigation of hydrocarbon chain packing in bilayers of polyunsaturated phospholipids. *Lipids.* 31:S199–S203.

Hoover, W. G. 1985. Canonical dynamics: equilibrium phase-space distributions. *Phys. Rev. A.* 31:1695–1697.

Huang, P., J. J. Perez, and G. H. Loew. 1994. Molecular dynamics simulations of phospholipid bilayers. *J. Biomol. Struct. Dyn.* 11: 927–956.

Jorgensen, W. L. 1986. Optimized intermolecular potential functions for liquid alcohols. *J. Phys. Chem.* 90:1276–1284.

Jorgensen, W. L. 1994. BOSS. Yale University, New Haven, CT.

Jorgensen, W. L., J. Chandrasekhar, J. D. Madura, R. W. Impey, and M. L. Klein. 1983. Comparison of simple potential functions for simulating liquid water. *J. Chem. Phys.* 79:926–935.

Litman, B. J., and D. C. Mitchell. 1996. A role for phospholipid polyunsaturation in modulating membrane protein function. *Lipids.* 31: S193–S197.

MacKerell, A. D., Jr., and M. Karplus. 1991. Importance of attractive van der Waals contributions in empirical energy function models for the heat of vaporization of polar liquids. *J. Phys. Chem.* 95:10559–10560.

Merz, K., and B. Roux, editors. 1996. Biological Membranes: A Molecular Perspective from Computation and Experiment. Birkhäuser, Boston.

Nagle, J. F., R. Zhang, S. Tristram-Nagle, W. Sun, H. Patrache, and R. Suter. 1996. X-ray structure determination of L_a phase DPPC bilayers. *Biophys. J.* 70:1419–1431.

Nakahara, S., and H. Masamoto. 1990. Interfacial tension of two-phase water-alkene binary liquid system. *J. Chem. Eng. Jpn.* 23:94–95.

Pascher, I., M. Lundmark, P. G. Nyholm, and S. Sundell. 1992. Crystal structures of membrane lipids. *Biochim. Biophys. Acta.* 1113:339–373.

Pastor, R. W. 1994. Molecular dynamics and Monte Carlo simulations of lipid bilayers. *Curr. Opin. Struct. Biol.* 4:486–492.

Pastor, R. W., and S. E. Feller. 1996. Time scales of lipid dynamics and molecular dynamics. *In* Biological Membranes: A Molecular Perspective from Computation and Experiment. K. Merz and B. Roux, editors. Birkhäuser, Boston. 3–29.

Pearce, L., and S. C. Harvey. 1993. Langevin dynamics studies of unsaturated phospholipids in a membrane environment. *Biophys. J.* 65: 1084–1092.

Reiher, W. E., III. 1985. Theoretical Studies of Hydrogen Bonding. Ph.D. thesis, Department of Chemistry, Harvard University, Cambridge, MA.

Ryckaert, W. E., G. Ciccotti, and H. J. C. Berendsen. 1977. Numerical integration of the cartesian equations of motion of a system with constraints: molecular dynamics of *n*-alkanes. *J. Comput. Phys.* 23: 327–341.

Schlenkrich, M., J. Brickmann, A. D. MacKerell, and M. Karplus. 1996. Empirical potential energy function for phospholipids: criteria for parameter optimization and applications. *In* Biological Membranes: A Molecular Perspective from Computation and Experiment. Birkhäuser, Boston. 31–81.

Seelig, J., and P. Macdonald. 1987. Phospholipids and proteins in biological membranes. ^{2}H NMR as a method to study structure, dynamics, and interactions. *Acc. Chem. Res.* 20:221–228.

Seelig, J., and N. Wasepe-Sarcevic. 1978. Molecular order in *cis* and *trans* unsaturated phospholipid bilayers. *Biochemistry.* 17:3310–3315.

Small, D. M. 1986. The Physical Chemistry of Lipids: From Alkanes to Phospholipids. Plenum Press, New York.

Tobias, D. J., K. Tu, and M. L. Klein. 1997. Atomic-scale molecular dynamics simulations of lipid membranes. *Curr. Opin. Colloid Interface Sci.* 2:115–26.

Tristram-Nagle, S., R. Zhang, R. M. Suter, C. R. Worthington, W. J. Sun, and J. F. Nagle. 1993. Measurment of chain tilt angle in fully hydrated bilayers of gel phase lecithins. *Biophys. J.* 64:1097–1109.

Weast, R. C., editor. 1976–1977. Handbook of Chemistry and Physics, 57th Ed. CRC Press, Boca Raton, FL.

Wiener, M. C., G. I. King, and S. H. White. 1991. Structure of a fluid dioleoylphosphatidylcholine bilayer determined by joint refinement of x-ray and neutron diffraction data. I. Scaling of neutron data and the distributions of double bonds and water. *Biophys. J.* 60:568–576.

Wiener, M. C., and S. H. White. 1991a. Fluid bilayer structure determination by the combined use of x-ray and neutron diffraction data. I. Fluid bilayer models and the limits of resolution. *Biophys. J.* 59:162–173.

Wiener, M. C., and S. H. White. 1991b. Fluid bilayer structure determination by the combined use of x-ray and neutron diffraction data. II. The "composition space" refinement method. *Biophys. J.* 59:174–185.

Wiener, M. C., and S. H. White. 1991c. The transbilayer distribution of bromine in fluid bilayers containing a specifically brominated analog of dioleoylphosphatidylcholine. *Biochemistry.* 30:6997–7008.

Wiener, M. C., and S. H. White. 1992a. Structure of a fluid dioleoylphosphatidylcholine bilayer determined by joint refinement of x-ray and neutron diffraction data. II. Distribution and packing of terminal methyl groups in a fluid lipid bilayer. *Biophys. J.* 61:428–433.

Wiener, M. C., and S. H. White. 1992b. Structure of a fluid dioleoylphosphatidylcholine bilayer determined by joint refinement of x-ray and neutron diffraction data. III. Complete structure. *Biophys. J.* 61: 434–447.

Yin, D., and A. D. MacKerell, Jr. 1996. Ab initio calculations on the use of helium and neon as probes of the van der Waals surfaces of molecules. *J. Phys. Chem.* 100:2588–2596.

Yin, D., and A. D. MacKerell, Jr. 1997. Combined *ab initio*/empirical approach for the optimization of Lennard-Jones parameters. *J. Comp. Chem.* In press.

Zhang, Y., S. E. Feller, B. R. Brooks, and R. W. Pastor. 1995. Computer simulation of liquid/liquid interfaces. I. Theory and application to octane/water. *J. Chem. Phys.* 103:10252–10266.